Fourier plasmonics: Diffractive focusing of in-plane surface plasmon polariton waves

Liang Feng,[a] Kevin A. Tetz, Boris Slutsky, Vitaliy Lomakin, and Yeshaiahu Fainman
Department of Electrical and Computer Engineering, University of California, San Diego, California 92093

(Received 29 June 2007; accepted 27 July 2007; published online 20 August 2007)

An in-plane Fresnel zone plate (FZP) for focusing surface plasmon polariton (SPP) fields has been designed, fabricated, and tested. The fabricated device consists of 400 nm tall by 5 μm wide amorphous Si-based SPP FZP on an Al film integrated with a pair of two-dimensional nanohole arrays for excitation of the incident and detection of the diffracted SPP fields. Diffracted SPP fields from each Fresnel zone constructively interfere at the expected focal point to produce focusing with threefold intensity enhancement. Temporal and spatial characteristics of the focused SPP fields are studied with time-resolved spatial-heterodyne imaging technique. Good agreement with average power measurements is demonstrated. Diffractive focusing of SPP fields, based on Fourier plasmonics, represents an approach to SPP in-plane microscopy. © *2007 American Institute of Physics*. [DOI: 10.1063/1.2772756]

Surface plasmon polaritons (SPPs) are electromagnetic surface waves formed through strong interaction between electromagnetic field and free electron oscillations at a metal-dielectric interface.[1] One unique property of the SPPs is their high confinement near the interface and intrinsically localized in a small volume, recently utilized in optical devices for subwavelength electromagnetic waveguiding, label-free biochemical sensing, nanophotolithography, and data storage.[2,3] SPP-based *S* bends, *Y* splitters, Mach-Zehnder interferometers, and waveguide-ring resonators have also been demonstrated.[4,5] Additionally, SPP wavelength can be shorter than the wavelength of light in surrounding media, leading to applications in subdiffraction-limited in-plane microscopy. Subdiffraction-limited imaging can, in principle, be realized by negative refractions to recover the high spatial frequency information carried by the evanescent wave.[6] However, in-plane SPP microscopy offers, arguably, a more promising alternative to accomplish this goal due to the challenge in fabricating negative refraction materials in the visible spectrum. In the past, far-field microscopy combined with the in-plane image magnification by SPP was suggested.[7] More recently, a negative refraction SPP hyperlens was implemented with resolution on the order of $\lambda_0/7$, far beyond the diffraction limit.[8] However, the challenge remains to excite and control propagating SPP fields in a systematic fashion as is possible with optical fields both in free space and dielectric waveguides. For example, it would be of great interest in biomedical research to create a confocal microscope with subdiffraction-limited resolution exploiting focused SPP fields.

To date, several groups have demonstrated schemes for SPP focusing. A converging SPP wave has been obtained by coupling a laser beam to SPP via an array of concentrically arranged circular metallic slits,[9,10] other in-plane structures,[11,12] or by coupling a converging beam via a two-dimensional rectangular nanohole array.[13] SPPs have also been localized at the sharp end of a tapered plasmonic waveguide.[14–16] Other authors have used refractive elements (e.g., a traditional lens[17] or a negative refraction superlens[18]) placed directly on top of the metallic film to focus SPP waves by introducing quadratic phase. In this letter, we report another focusing approach using an in-plane SPP Fresnel zone plate (FZP).[19] We provide design rules for the construction of such a FZP and demonstrate experimentally the diffractive focusing of SPP fields in the plasmonic structures fabricated according to these design rules.

A conventional optical binary amplitude FZP consists of a series of concentric rings, known as Fresnel zones that alternate in transmittance between transparent (i.e., 1) and opaque (i.e., 0). An adaptation of FZP for in-plane SPP focusing is illustrated schematically in Fig. 1(a). Consider the diffraction of a SPP plane wave impinging on this structure from the left. Constructive interference of SPP fields is obtained at a focal distance f from the FZP when Fresnel zone radii r_m satisfy

$$r_m = \sqrt{m\lambda_{\mathrm{SPP}} f + \frac{m^2\lambda_{\mathrm{SPP}}^2}{4}}, \tag{1}$$

where m is an integer and λ_{SPP} is the SPP wavelength. For a planar FZP, r_m are boundary positions where transmittance changes between transparent and opaque. In our experiments, a 12-zone SPP FZP with zone radii given by Eq. (1) was constructed at an Al/air interface for operation at a free space wavelength of 1.55 μm (corresponding to $\lambda_{\mathrm{spp}}=1.547$ μm) and a focal length $f=80$ μm. As in previous

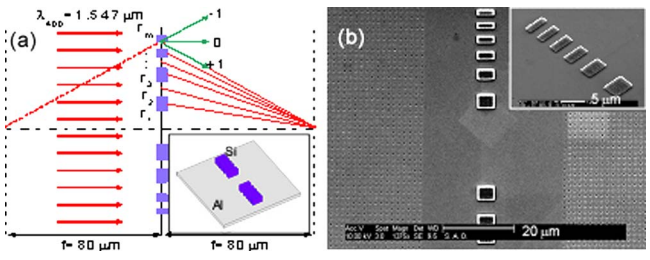

FIG. 1. (Color online) (a) Schematic diagram of SPP FZP geometry and design parameters; (b) SEM micrographs of SPP FZP fabricated by deposition of amorphous Si on Al/air interface; Also seen are the integrated arrays of nanoholes in the Al film for SPP field excitation (left) and detection (right).

[a]Electronic mail: lifeng@ucsd.edu

work,[13,20] nanohole arrays were integrated on both sides of the device for launching SPP waves and visualizing their propagation.

The sample was fabricated by standard e-beam lithography as follows: (i) a glass substrate was first cleaned and then coated with 5 nm thick Ti and 100 nm thick Al films; (ii) a 1.5 μm thick polymethyl methacrylate (PMMA) layer was spun onto the metal plate and 5 μm wide FZP features were defined in PMMA by e-beam writing; (iii) a 400 nm thick film of amorphous Si was deposited over the PMMA mask; (iv) using acetone lift-off procedure, the Si-based FZP was formed on the Al film surface; (v) the entire sample was covered again with a 200 nm thick PMMA layer for the fabrication of two nanohole arrays, one to the left and the other to the right of the SPP FZP; (vi) the PMMA was e-beam patterned to create 200×200 μm^2 nanohole arrays on a 1.6 μm square grid and with average nanohole diameter of 300 nm; and (vii) the nanohole arrays were transferred to the Al film by wet chemical etching (E6 Metal Etchant), and PMMA was then removed using acetone. Scanning electron microscopy (SEM) micrographs of the final product, showing the FZP and both nanohole arrays on the Al film, are reproduced in Fig. 1(b).

The fabricated device was tested with our time-resolved spatial heterodyne imaging technique based on a modified Mach-Zehnder interferometer operating with mode-locked 200 fs ultrashort laser pulses at a center wavelength of 1.55 μm.[13] Incident light was polarized at 45° to the nanohole arrays, and reradiated field was detected with an orthogonally oriented polarization analyzer.[13,20] Laser light was focused through a 5× microscope objective onto the input nanohole array to the left of the FZP at normal incidence. The lattice constant of hole arrays was chosen close to the SPP wavelength so that $[\pm1, 0]$ and $[0, \pm1]$ SPP modes were excited, with [1,0] mode directed toward the FZP. The incident SPP was converging at a half angle of 2°, negligible compared to the 27° convergence half angle introduced by the FZP. (The alignment of the objective was verified using a different area of the same sample.) The excited SPP wave had a transverse width of about 80 μm. Diffraction at the SPP FZP and subsequent interference resulted in focusing of the transmitted SPP at a particular location in the area of the output nanohole array to the right of the FZP. This detection nanohole array caused SPP to radiate into far field, where an image was finally captured with a 10× microscope objective coupled to a charge-coupled device camera. The result of this measurement, shown in Fig. 2(a), represents the intensity map of SPP over the output nanohole array. The + first-order FZP focal point is clearly seen at $x=-27$ μm, 83 μm away from the FZP (located outside the image at $x=-110$ μm, 20 μm to the left of the white dashed line indicating the edge of the nanohole array). The 83 μm measured focal length is in good agreement with the 80 μm expected from Eq. (1). Fringes due to the diverging − first-order of the FZP are also visible.

The intensity map in Fig. 2(a) also reveals the rapid attenuation of SPP waves as they propagate from left to right across the nanohole array. The second nanohole array is introduced only for visualization purposes and, in principle, would not be necessary in in-plane imaging applications. It is therefore informative to compensate for the radiation losses caused by this array in post processing. To this end, we assumed that, absent radiation and material loss, the SPP's energy flow would be conserved, i.e., the integration of the measured intensity of the scattered SPP waves along the y direction would be the same at different x locations. Then the calculated material loss of Al (SPP propagation length of ~322.5 μm at 1.55 μm wavelength[1]) was added back to show the SPP intensity map predicted without the radiation loss in the area of the detection nanohole array. It is seen in Fig. 2(b) that, if the detection nanohole array is not present, SPP intensity at the focal point may be expected to be about three times that of the input SPP wave.

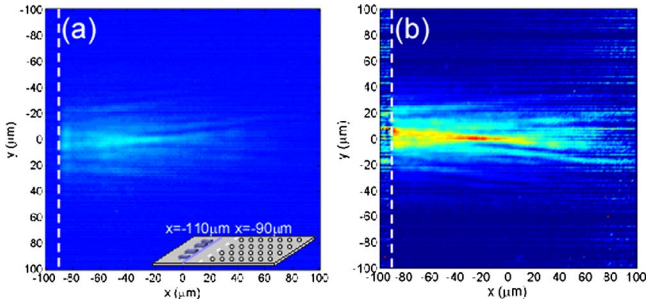

FIG. 2. (Color online) (a) Measured SPP time-averaged intensity map over the nanohole array to the right of the FZP, showing + first-order diffractive focusing and − first-order diffractive fringes. Dashed white line indicates the left edge of the nanohole array. The FZP is located at $x=-110$ μm. Inset: schematic diagram of the FZP and the nanohole array. (b) Postprocessed image obtained from (a) by compensating for radiative loss.

The effectiveness of the in-plane SPP FZP described in this letter is limited somewhat by the fact that even its opaque zones are partially transparent. This is due to the technical difficulty of fabricating Si-based FZP higher than several microns using the lift-off method. The evanescent tail of SPP fields in air extends further than the height of the FZP, and therefore a fraction of the incident SPP fields is transmitted through the FZP opaque zones. Consequently, part of the SPP "sails over" the Si barrier. Experimentally, about 30% transmission was observed through the "opaque" zones, a figure consistent with our finite-element numerical models. This defect can be taken into account by generalizing the standard expression for FZP diffracted field[19] to include contributions from both the transparent and the opaque zones,

$$u(x,y)=\frac{\exp(ik_{\mathrm{SPP}}x)}{i\lambda_{\mathrm{SPP}}x}\int_T\int u_0(y_0)\exp\left(\frac{ik_{\mathrm{SPP}}}{2x}(y-y_0)^2\right)dy_0 + \frac{\exp(ik_{\mathrm{SPP}}x)}{i\lambda_{\mathrm{SPP}}x}\int_O\int \sqrt{0.3}u_0(y_0) \times\exp\left(\frac{ik_{\mathrm{SPP}}}{2x}(y-y_0)^2\right)dy_0. \quad (2)$$

SPP intensity $|u(x,y)|^2$ at the focal plane ($f=80$ μm) calculated from Eq. (2) is plotted in Fig. 3(a), and agrees well with the measured data in Fig. 3(b). Methods of conventional Fourier optics can thus be applied to describe in-plane diffraction of SPP waves. The reasons for the small discrepancy probably include the error of Fresnel approximation due to steep focusing geometry, and the rough estimate of the transparency of the opaque FZP zones.

In addition to average power measurement (Figs. 2 and 3), temporal-spatial amplitude distributions of the SPP waves were investigated with our time-resolved spatial heterodyne imaging technique.[13] Interference patterns between a reference beam and far-field radiation of SPP passing over the

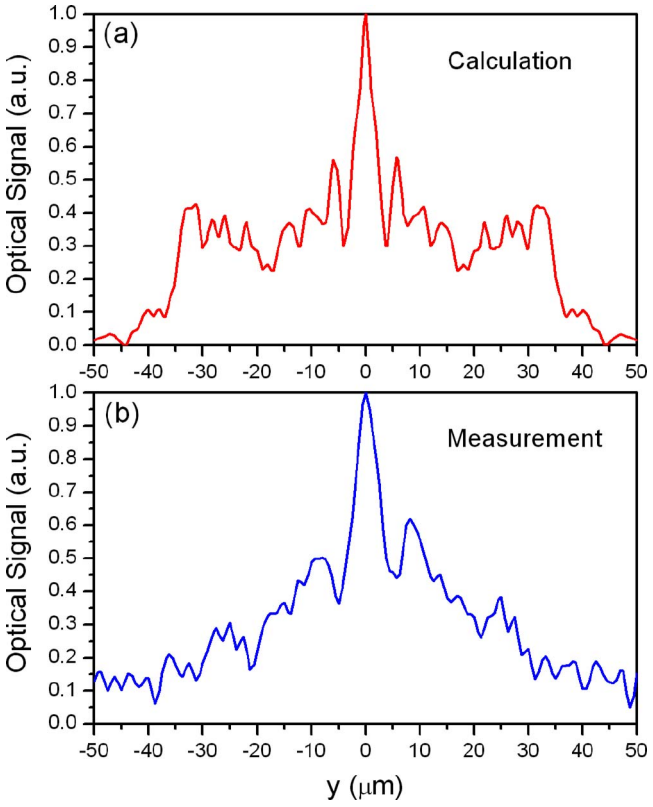

FIG. 3. (Color online) SPP intensity profile in the focal plane computed by the Fresnel diffraction method (a) and found experimentally (b).

nanohole array were captured at 150 different time delays, with about 6 fs separation between adjacent frames. Figures 4(a)–4(c) show field magnitude spatial maps at times $\tau=0$, 220, and 650 fs. Propagation of the SPP wave packet from left to right over time is clearly visualized. The packet is also seen to converge to the optical axis at the focal point and diverge again thereafter. We also observed that the SPP focal spot can be moved by slight adjustment of the angle of incidence and the quadratic phase of the incident laser beam. This phase-controlled strategy can be helpful for in-plane microscopy applications.

In summary, an in-plane FZP for diffractive focusing of SPP fields on an Al/air interface was designed and fabricated. In-plane diffractive focusing of SPP was demonstrated and quantitatively characterized. The temporal and spatial characteristics of the focused SPP fields were experimentally analyzed using time-resolved spatial-heterodyne imaging technique. The measured time-resolved spatial amplitude images provide additional insight and confirm both the analysis and the measured average power results. The FZP focused SPP fields down to a focal point on a flat metallic film surface and concentrated the incident power of the SPP. This power concentration may help improve the contrast and longitudinal resolution of SPP in-plane microscopy, as well as facilitate interesting SPP-based nonlinear effects such as surface enhanced Raman scattering.[15] In addition to the refractive plasmonics,[17] our work on SPP diffraction leads to a direction of research on Fourier Plasomics.

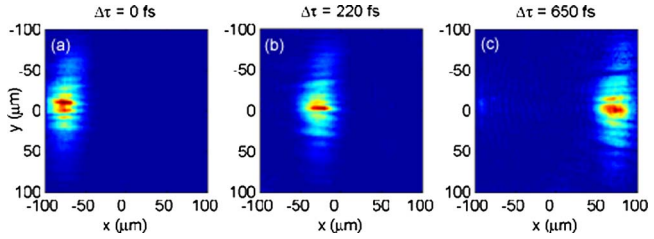

FIG. 4. (Color online) Temporal evolution of spatial amplitude of the scattered SPP fields from the detection nanohole array (ranging from $x=-100$ μm to $x=100$ μm). (a) The converging SPP wave observed when the SPP pulse just enters the hole array. (b) The SPP pulse reaching its focal point after about 220 fs. (c) The SPP pulse diverging past the focal point.

Authors would like to thank L. Pang, and H.C. Kim in UCSD as well as Xin Heng from Caltech for helpful discussions in fabrication. This work is supported by NSF, DARPA, and Center for Optofluidic Integration

[1] H. Raether, *Surface Plasmons on Smooth and Rough Surfaces and on Gratings* (Springer, Berlin, 1988), pp. 4–7.
[2] W. L. Barnes, A. Dereux, and T. W. Ebbesen, Nature (London) **424**, 824 (2003).
[3] E. Ozbay, Science **311**, 189 (2006).
[4] S. I. Bozhevolnyi, V. S. Volkov, E. Devaux, J.-Y. Laluet, and T. W. Ebbesen, Nature (London) **440**, 508 (2006).
[5] V. S. Volkov, S. I. Bozhevolnyi, E. Devaux, J.-Y. Laluet, and T. W. Ebbesen, Nano Lett. **7**, 880 (2007).
[6] J. B. Pendry, Phys. Rev. Lett. **85**, 3966 (2000).
[7] I. I. Smolyaninov, J. Elliott, A. V. Zayats, and C. C. Davis, Phys. Rev. Lett. **94**, 057401 (2005).
[8] I. I. Smolyaninov, Y.-J. Hung, and C. C. Davis, Science **315**, 1699 (2007).
[9] Z. W. Liu, J. M. Steele, W. Srituravanich, Y. Pikus, C. Sun, and X. Zhang, Nano Lett. **5**, 1726 (2005).
[10] Z. W. Liu, J. M. Steele, H. Lee, and X. Zhang, Appl. Phys. Lett. **88**, 171108 (2006).
[11] L. Yin, V. K. Vlasko-Vlasov, J. Pearson, J. M. Hiller, J. Hua, U. Welp, D. E. Brown, and C. W. Kimball, Nano Lett. **5**, 1399 (2005).
[12] R. Kiyan, C. Reinhardt, S. Passinger, A. L. Stepanov, A. Hohenau, J. R. Krenn, and B. N. Chichkov, Opt. Express **15**, 4205 (2007).
[13] R. Rokitski, K. A. Tetz, and Y. Fainman, Phys. Rev. Lett. **95**, 177401 (2005).
[14] M. I. Stockman, Phys. Rev. Lett. **93**, 137404 (2004).
[15] E. Verhagen, L. Kuipers, and A. Polman, Nano Lett. **7**, 334 (2007).
[16] K. Li, X. Li, M. I. Stockman, and D. J. Bergman, Phys. Rev. B **71**, 115409 (2005).
[17] A. Hohenau, J. R. Krenn, A. L. Stepanov, A. Drezet, H. Ditlbacher, B. Steinberger, A. Leitner, and F. R. Aussenegg, Opt. Lett. **30**, 893 (2005).
[18] H. Shin and S. Fan, Phys. Rev. Lett. **96**, 073907 (2006).
[19] J. W. Goodman, *Introduction to Fourier Optics*, 2nd ed. (McGraw-Hill, New York, 1996), p. 124.
[20] K. A. Tetz, R. Rokitski, M. Nezhad, and Y. Fainman, Appl. Phys. Lett. **86**, 111110 (2005).